



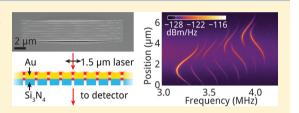
pubs.acs.org/journal/apchd5

Parallel Transduction of Nanomechanical Motion Using Plasmonic Resonators

Rutger Thijssen,[†] Tobias J. Kippenberg,[‡] Albert Polman,[†] and Ewold Verhagen*,[†]

[†]Center for Nanophotonics, FOM Institute AMOLF, Science Park 104, 1098XG Amsterdam, The Netherlands

ABSTRACT: We demonstrate parallel transduction of thermally driven mechanical motion of an array of gold-coated silicon nitride nanomechanical beams, by using near-field confinement in plasmonic metalinsulator-metal resonators supported in the gap between the gold layers. The free-space optical readout, enabled by the plasmonic resonances, allows for addressing multiple mechanical resonators in a single measurement. Light absorbed in the metal layer of the beams modifies their mechanical properties, allowing photothermal tuning of the



eigenfrequencies. The appearance of photothermally driven parametric amplification indicates the possibility of plasmonic mechanical actuation.

KEYWORDS: plasmonics, optomechanics, near-field interactions, photothermal force, NEMS arrays, nano-optomechanical transducers

rrays of nanomechanical resonators have many applica-A tions, ranging from force and mass sensing^{1,2} to collective nonlinear dynamics³ and mechanical memories and computing.4 In particular, large numbers of integrated mechanical sensors can enable sensitive, rapid, label-free, and massively parallel detection of biochemical species and trace gases.^{5,6} By varying the frequency of the oscillators in an array, the sensing bandwidth can be effectively increased. Parallelization can also address some of the difficulties associated with scaling down mechanical oscillator size, which is generally favorable for sensitivity: difficulties that include reduced power handling capability^{7,8} and reduced effective interaction cross section (i.e., the sensor surface area). Another challenge that nanoscale mechanical systems pose is how to efficiently transduce mechanical motion to a measurable signal, crucial to any sensor's operation. In the case of a sensor consisting of multiple mechanical oscillators, it is often useful to create a system that can be measured using a single input and single output,9 by separating the oscillators in frequency. Mechanical arrays have been demonstrated using various readout schemes: electrical readout, 10 using optical diffraction, 11 and using (deformable) optical waveguides. 12

Here, we demonstrate the parallel transduction of the motion of an array of nanobeams using a single laser beam focused on the array. The transduction is mediated by surface plasmon Fabry-Pérot resonances in the narrow metal-coated slots between the nanobeams. We show how this principle 13,14 can be extended to measuring individual mechanical resonator modes in an array of nanobeams. We use metal-dielectricmetal plasmon resonances, which are very sensitive to the width of the dielectric region.¹⁵ Motion of the oscillator then changes the plasmonic configuration, thus changing the transmission of the cavity.

The small size of plasmonic resonators allows high mode overlap with nanomechanical modes. At the same time, the free-space addressability of localized surface plasmon resonances allows the use of simple optical elements to couple light to and from the cavity, without having to resort to for instance nanoscale positioning of waveguides, as is necessary for many photonic crystal cavity¹⁶ and microcavity¹⁷ optomechanical implementations. This free-space addressability makes measuring multiple mechanical oscillators with a single laser beam a relatively straightforward process.

During the measurement, the beams absorb some of the incident light. We demonstrate that this leads to photothermal modification of the beams' eigenfrequencies. 18-21 We discuss the induced mechanical coupling between the nanobeams. At high enough driving powers, the photothermal heating can parametrically amplify the motion of the beams. This photothermal amplification effect has been observed in a variety of optomechanical systems: in metal-coated cantilevers, 22,23 in semiconductor membranes using electron-hole pair relaxation,²⁴ and in microdisks.²⁵ Photothermoelastic interactions may thus allow for both tuning and actuation in these systems.

EXPERIMENTAL METHODS

To fabricate arrays of parallel mechanical nanobeams, 110 nm of gold is sputter coated on commercially available high-stress stoichiometric silicon nitride membranes of 50 nm thickness (Norcada, Canada). Using a focused ion beam (30 keV Ga+ ions, current 10 pA), we mill nine 18- μ m-long slits in a single pass, creating eight nanomechanical beams, each separated by a slit width of 20 nm. The beam widths are fabricated to range in

Received: July 21, 2014 Published: October 7, 2014



[‡]École Polytechnique Fédérale de Lausanne (EPFL), Lausanne, Switzerland

incrementing steps from 475 to 550 nm wide. The difference in beam widths lifts the degeneracy of the in-plane eigenfrequencies and allows the identification of individual beams from the transduced mechanical spectrum. The out-of-plane mechanical eigenfrequencies are to first order independent of beam width and are therefore more difficult to separate spectrally. However, the out-of-plane and in-plane eigenmodes are well separated in frequency (~2.2 and ~3.7 MHz, respectively), and we will mostly consider the latter below.

Figure 1a shows a scanning electron microscopy (SEM) image of the fabricated array, taken with the gold-coated side of

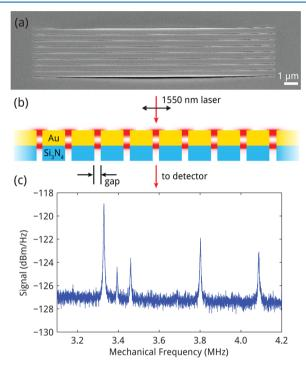


Figure 1. Experimental geometry. (a) SEM micrograph of array structure, tilted at 52°, taken on the gold side of an array of eight parallel microbeams (beam length: 18 μ m; thickness: 50 nm Si₃N₄, 110 nm Au; beam widths: 475 to 550 nm; gap width: 20 nm). (b) Schematic cross section of the nanomechanical beam array. Red spots indicate plasmonic Fabry–Pérot resonances excited in the slits between the Au layers by a 1550 nm CW laser. (c) Frequency spectrum of light intensity transmitted through the array, showing five distinct resonances caused by five of eight nanomechanical beams in the array.

the membrane upward and the sample tilted at 52°. The narrow gaps between the nanobeams are clearly visible; a larger gap is seen for the two outer sides, where the silicon nitride membrane bends downward due to its in-plane stress.

The sample is then placed in a custom-built confocal transmission microscope, which resides inside a vacuum chamber that is evacuated to 10^{-3} mbar to reduce viscous air drag on the nanobeams. A 1550 nm wavelength CW erbium-doped fiber laser is focused onto the sample, polarized orthogonal to the slits, and incident from the gold-coated side of the nanobeams, as shown in the schematic cross section in Figure 1b. Different focusing conditions were used, as will be described later on.

NANOMECHANICAL TRANSDUCTION

Mechanical displacement affects the optical response of the slots, changing the transmitted power. In the present geometry, the motion of eight parallel nanobeams is measured simultaneously. Figure 1c shows the frequency spectrum measured by defocusing the laser beam to a spot diameter of $\sim 5~\mu m$, so that all plasmonic gaps are illuminated, and detecting a power of approximately 12 μW . The peaks are related to the thermal motion of individual mechanical modes. Interestingly, only five resonant mechanical modes are observed in the spectrum, with varying amplitude. To analyze this, we first discuss how the motion of the eight beams is transduced to the measured intensity.

The motion of each of the beams is probed by its two adjacent slits, each of which supports a plasmonic resonance. The transmitted power through each slit can be written as $\eta(d_i)\mathcal{P}_i$, where \mathcal{P}_i is the optical power density (in W/m²) interacting with slit i and $\eta(d)$ is an effective scattering cross section into the transmission channel, which is a function of the slit width d_i .

For in-plane motion, the two slits at either side of the beam have widths $d_1(x)=\overline{d}_1+x$ and $d_2(x)=\overline{d}_2-x$, respectively, where \overline{d}_i denotes the mean width of slit i, and x is the displacement of the beam (we take the mean displacement $\overline{x}=\langle x(t)\rangle=0$). The total transmitted power is, as such, $T=\eta(\overline{d}_1+x)\mathcal{P}_1+\eta(\overline{d}_2-x)\mathcal{P}_2$. This power is modulated through oscillations of the beam, as to first (linear) order

$$\frac{\mathrm{d}T}{\mathrm{d}x} = \frac{\mathrm{d}\eta}{\mathrm{d}x} (\overline{d}_1) \mathcal{P}_1 - \frac{\mathrm{d}\eta}{\mathrm{d}x} (\overline{d}_2) \mathcal{P}_2 \tag{1}$$

For a plane wave incident on a nanobeam surrounded by two identical slits, this would lead to completely vanishing transduction of motion as $\overline{d}_1 = \overline{d}_2$ and $\mathcal{P}_1 = \mathcal{P}_2$. Figure 2a shows a schematic of this geometry. An SEM image of such an array is shown in Figure 2c. This equation can be expanded to include the shape of the mechanical mode, by integrating along the length of the beam, weighting the integral by the laser intensity along the beam length. This will lead to a linear correction factor for eq 1.

So far, we considered only the slits immediately adjacent to the moving beam to contribute to transduction. While transduction through these two slits is likely dominating, it is in principle possible that the slits are optically coupled, leading to transduction involving other slits. We note that even for interacting slits the symmetry of the system and its illumination dictate that transduction vanishes for equal slit widths, if the total size of the array exceeds the typical coupling length. Assuming an array of slits, labeled from -i to i, the transmission through slit i is a function of the slit's polarizability $\mathbf{p}_i(x)$. With the incoming beam centered on the array, we have $\mathbf{p}_i(x) =$ $\mathbf{p}_{-i}(-x)$, if x denotes the in-plane displacement of the middle beam. This leads to a change in polarizability $(d/dx)\mathbf{p}_i(x) = (d/dx)\mathbf{p}_i(x)$ dx) $\mathbf{p}_{-i}(-x) = -(d/dx)\mathbf{p}_{-i}(x)$. The total transmitted field is then $T \propto \sum_{i} \sum_{j} p_{i} p_{j}^{*}$. Working out the terms in this equation for a modulation of the widths d_{-i} , d_i of the center two slits leads to (dT/dx) = 0.

Two factors can potentially break down this expectation and lead to a resonance peak: (1) a different input power density $\mathcal P$ on the two slits, due to the fact that a nonuniform (for instance, a focused) beam is used, and (2) a difference in slit widths $\overline{d}_1 \neq \overline{d}_2$. Because the plasmonic coupling strength depends on

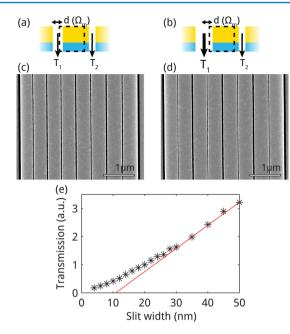


Figure 2. Parallel mechanical transduction. Schematic of transduction through (a) constant-width and (b) alternating-width gaps. SEM micrographs of center of arrays of (c) constant-width gap (20 nm) and (d) alternating-width gap (20 and 50 nm) array structures. (e) Transmission through slit as a function of slit width *d*, extracted from FDTD simulations. The red line is a linear fit to the transmission through slits of width greater than 35 nm.

the slit width, η is not linearly dependent on d, such that $(\mathrm{d}\eta/\mathrm{d}x)(\overline{d}_1) \neq (\mathrm{d}\eta/\mathrm{d}x)(\overline{d}_2)$ if $\overline{d}_1 \neq \overline{d}_2$. This implies that by changing the width of the slit on either side of a beam we can allow transduction of motion to transmitted power. Importantly, it is the nonlinear dependence of slit transmission η on slit width d (or on slit area, for that matter) that is crucial to allow transduction. Such a nonlinear dependence on slit width, shown in Figure 2e, is a defining characteristic of plasmonic response. In this figure, the black data points are the transmission extracted from a series of FDTD simulations of slits of differing widths. The transmission is normalized to the transmission through the 20-nm-wide slit. The red line is a linear fit to slits of widths between 35 and 100 nm, showing the nonlinear behavior of the plasmonic transmission for slit widths narrower than 30 nm.

In the structure of Figure 1 differences between slit widths are caused by fabrication imperfections, allowing observation of the motion of some of the beams in Figure 1c. The outermost slits in the structure are much wider: in-plane stress in the silicon nitride causes bending in the membrane surrounding the array structure, leading to a resonance peak for the two outermost beams. For some of the inner beams, the surrounding slits are also slightly different.

Next, we study the transduction for an an array in which the slits were intentionally made alternately narrow (20 nm) and wide (50 nm), shown schematically in cross section in Figure 2b and in an SEM image in Figure 2d. For these structures, we expect that $(\mathrm{d}\eta/\mathrm{d}x)(\overline{d}_1) \neq (\mathrm{d}\eta/\mathrm{d}x)(\overline{d}_1)$ for all beams, based on finite-difference-time-domain simulations of metal–insulator–metal slits of varying width (Figure 2e). Therefore, the motion of all beams is expected to be transduced. At the laser wavelength of 1550 nm, we find from the FDTD simulations that $(\mathrm{d}\eta/\mathrm{d}x)(20 \text{ nm}) = 0.75(\mathrm{d}\eta/\mathrm{d}x)(50 \text{ nm}).^{14}$

We again measured the transduction with a defocused beam and simultaneously detected the modulations induced by eight beams with widths ranging from 475 to 525 nm. This time, we achieve parallel transduction of motion of all eight beams, as shown in Figure 3, when we detect a power of 15 μ W. Note

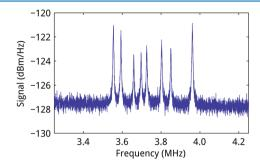


Figure 3. Frequency spectrum of light transmitted through an array with eight beams, with alternating-width slits of 20 and 50 nm, with beam widths ranging from 475 to 525 nm. The laser beam was defocused to a spot size of \sim 5 μ m.

that the signal-to-noise ratio is limited by the modest mechanical quality factor (typically Q < 1000) in this proof-of-principle demonstration. The mechanical quality factor can be straightforwardly improved by reducing the amount of gold near the beam ends. We have now seen that using alternate slit widths (20 and 50 nm) is a viable method to enable parallel transduction of the motion of eight parallel resonators using a single focused laser beam.

To further investigate the transduction of each beam by its two neighboring slits, we perform measurements in which both structures were scanned through the focus of a laser beam (2.48 \pm 0.06 $\mu \rm m$ fwhm for the constant-width array, 2.84 \pm 0.13 $\mu \rm m$ for the alternating-width array), scanning orthogonal to the long axis of the beams. Figure 4a and b show color plots of the spectral density of transduced power as a function of the position of the laser beam across the constant-gap-width and alternate-gap-width arrays, respectively. Eight different curves are now clearly resolved for both structures, each corresponding to the motion of an individual nanobeam. Interestingly, as the laser beam is scanned across a single nanobeam, the mechanical resonance wavelength decreases and increases. This will be discussed further below.

Another striking feature in the transduction spectra in Figure 4a is that the intensity shows clear dips close to the center for all beams, except for the two outermost ones. The red data points in the subpanels of Figure 4c show the mechanical transduction power at resonance for each laser beam position. Each subpanel shows data for a single beam. The transduction curves clearly show dips in transduction for the six center beams when the focal spot is close to the center of each beam, when $\mathcal{P}_1 = \mathcal{P}_2$, implying a vanishing transduction, and showing that \overline{d} is very similar for the seven center slits. If the slits were all exactly equal in width, the shape of the dip should be proportional to the derivative of the spatial intensity profile of the laser spot on the sample. However, due to fabrication imperfections, the slits have slightly differing widths. We also attribute the transduction visible in Figure 1c to this. The mechanical transduction for each beam in the alternate-gapwidth array is plotted in Figure 4d. The dips in the transduction are now much less pronounced compared to those observed for the constant-width array shown in Figure 4a and c and are in

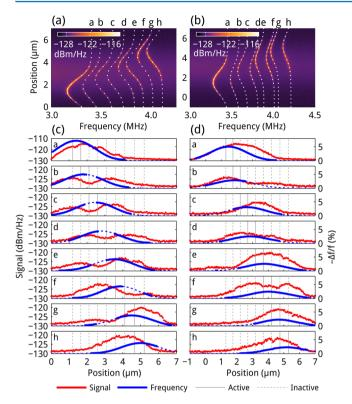


Figure 4. Mechanical resonance intensities. (a) Line scan across the center of an array of eight nanobeams separated by a fixed width of 20 nm. The peak resonance frequency is plotted on the horizontal axis, and the resonance peak intensity is represented by the color scale. Dots indicate Gaussian fits to peak frequencies as a function of the laser focus position on the array. (b) Similar to (a), for an array with beams alternately separated by 20 and 50 nm. (c) Transduction curves extracted from (a): the resonance peak intensities are shown as a function of laser spot position (red dots), along with the peak resonance frequencies (blue line). A dashed line indicates that the signal was too low to extract for use in fitting. The gray vertical lines indicate the positions of the slits, with the solid lines indicating the slits next to the beam for which the transduction is plotted. (d) Transduction curves extracted from (b). The focal diameters, 2.48 \pm 0.06 μ m fwhm for (a) and 2.84 \pm 0.13 μ m for (b), were determined from the average width of the Gaussian fits. Laser power detected was 11.5 μ W (a, c) and 10.5 μ W (b, d).

fact absent in most cases, showing that $(d\eta/dx)(50 \text{ nm}) \neq (d\eta/dx)(20 \text{ nm})$.

The measurements in Figures 3 and 4 provide direct proof that the transduction through the arrays is due to a plasmonic effect. If the transmission through the slits was simply due to a geometric effect, i.e., a transmission that is linearly proportional to the slit width, we would not observe any transduction of motion: for in-plane motion, the total width of the two slits surrounding a nanobeam is constant, and therefore no transduction would be expected. However, the plasmonic resonance mediating the transmission through the slit will lead to nonlinear dependence of transmission on slit width (as shown in Figure 2e), allowing the alternate-slit-width structure to improve transduction of the in-plane mechanical mode, and precludes the observed effects being due to a purely geometric modulation of the transmitted light by the beams' motion.

■ THERMAL TUNING OF EIGENFREQUENCIES

Figure 4 shows that the mechanical eigenfrequencies of the beams depend strongly on their position relative to the laser spot. We ascribe this to a photothermal effect: heating-induced expansion of the tensile-stressed beams causes a reduction in the axial stress, leading to reduced resonance frequencies. The maximum frequency shift is observed when the laser beam is centered on a nanobeam, where heating is maximum. We perform Gaussian fits to the (thermally shifted) resonance frequency as a function of laser focus position for each beam. The blue lines in the subpanels of Figure 4c and d show the thermally tuned frequency shift $\Delta f = (f_{\rm tuned} - f_0)/f_0$. Frequency shifts as high as 5% (150 kHz) are observed.

To further investigate this effect, we calculate the relative frequency shift as a function of absorbed power using a simple thermal model. We calculate the eigenfrequencies as a function of stress in the nitride layer of the beams:

$$f = \frac{1}{2\pi} \frac{\beta^2}{L^2} \sqrt{\frac{E_e I}{\rho_e wh} + \frac{12.30 \sigma_e L^2}{\rho_e \beta^4}}$$
 (2)

with L the length of the beam, w the width, h the thickness, and I the geometrical moment of inertia, and using geometric averaging to calculate the effective stress $\sigma_{\rm e}$, Young's modulus $E_{\rm e}$, and density $\rho_{\rm e}$ for the Au/Si₃N₄ bilayer beams. This geometric averaging is valid when most of the forces are along the length of the beams, implying that the system is far from buckling due to thermal stresses. As we are measuring the fundamental mode, we use $\beta = 4.730~04$. Note that all equations are also valid for single-layer beams.

To fit the model to the data, we first extract the nonthermally shifted eigenfrequencies f_i from the Gaussian fits in Figure 4a,b and plot these as a function of beam width in Figure 5a. We then fit eq 2 to the data using the effective Young's modulus $E_{\rm e}$ and stress $\sigma_{\rm e}$ as free parameters, using length and height as determined from SEM images and using literature values for the mass densities of gold and silicon nitride. Figure 5a shows good agreement between model and data for an effective Young's modulus of $E_{\rm e}=75.2$ GPa, between the value of that for gold and silicon nitride. We will assume the Young's moduli are independent of temperature. The fitted effective stress (in the low-power limit) is 36.5 MPa. Assuming the manufacturer's specification of $\sigma_{\rm e}=250$ MPa, this implies that there is a compressive stress of $\sigma_{\rm Au}=-60$ MPa in the gold layer.

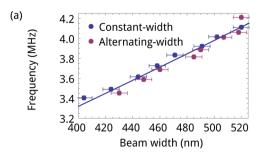
Next, we investigate the effect of heating of the nanobeams as they absorb light, changing the stress in the nanobeam through the thermal expansion coefficient:

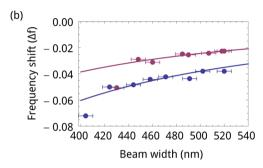
$$\sigma_{\rm e} = \sigma_{\rm i} + \sigma_{\rm t} = \sigma_{\rm i} - \alpha_{\rm e} E \Delta T \tag{3}$$

where σ_i is the original stress determined above, σ_t is the thermal stress, ΔT is the average temperature increase of the nanobeam, and α_e is the effective thermal expansion coefficient $\alpha_e = (\alpha_{\text{Si}_3\text{N}_4} A_{\text{Si}_3\text{N}_4} + \alpha_{\text{Au}} A_{\text{Au}})/(A_{\text{Si}_3\text{N}_4} + A_{\text{Au}})$, where $A_i = w_i \times h_i$ is the cross-sectional area of layer i. For this formulation for σ_e to be valid, we assume the end points of the beam do not move. We can then calculate the relative frequency change due to heating, using eq 2:

$$\delta f = \frac{\Delta f}{f} = \frac{f_{\rm t} - f_{i}}{f_{i}} = \sqrt{1 + \left(\frac{f_{0}}{f_{i}}\right)^{2} \frac{\sigma_{i} L^{2}}{3.4 E_{\rm e} w^{2}}} - 1 \tag{4}$$

where f_t is the thermally tuned frequency (eq 2 with σ from eq 3), f_i is the prestressed frequency without heating (eq 2 with σ_e





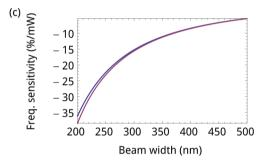


Figure 5. (a) Nonthermally shifted eigenfrequencies for constant-width array (blue data points derived from Figure 4a,c) and alternate-width array (red dots, derived from Figure 4b,d) and model, fitting effective Young's modulus $E_{\rm e}$ and in-plane stress $\sigma_{\rm e}$. (b) Measured thermally induced maximum frequency shifts from Figure 4 for constant-width (blue) and alternating-width (red) arrays as a function of beam width. The drawn lines are fits using eq 6, with the fraction of absorbed power γ as a free parameter. (c) Calculated frequency shift in %/mW of absorbed power for a gold-coated silicon nitride beam, plotted as a function of beam width. The purple line is for the alternating-width array; the blue line, for the constant-width array.

= σ_i), and f_0 is the eigenfrequency for a beam with no added stress ($\sigma_e = 0$).

We use a one-dimensional heating model, in which the beam is heated by a power $P_{\rm abs}$ applied evenly across the cross section of the beam at x_0 , while the ends of the beam are kept at ambient temperature (T(0) = T(L) = 298 K). In the stationary case, the absorbed power equals the outgoing fluxes:

$$P_{\text{abs}} = A\kappa (T(x_0) - T(0)) \left(\frac{1}{x_0} + \frac{1}{L - x_0} \right)$$
 (5)

with κ the heat conductivity, so that $\Delta T = P_{\rm abs} L/8\kappa A$. Using eqs 3–5, we find

$$\delta f = \sqrt{1 - \left(\frac{f_0}{f_i}\right)^2 \frac{\alpha_e L^3}{27.6\kappa_e w^3 h} P_{\text{abs}} - 1}$$
 (6)

The untuned frequencies f_0 and f_i are extracted from the Gaussian fits to the thermal tuning as shown in Figures 4 and

5a. Effective parameters for α and κ are derived from the weighted averages using $\alpha_{\rm Si_3N_4}=1.23\times 10^{-6}~{\rm K}^{-1}$, $\alpha_{\rm Au}=14\times 10^{-6}~{\rm K}^{-1}$, $\kappa_{\rm Si_3N_4}=2.5~{\rm W~m}^{-1}~{\rm K}^{-1}$, and $\kappa_{\rm Au}=320~{\rm W~m}^{-1}~{\rm K}^{-1}.^{20}$ That leaves the absorbed power $P_{\rm abs}$ to be directly determined from δf using eq 6.

Assuming the laser focus has a 2D Gaussian shape, the power density absorbed on one beam, with width w, can be expressed as a function of the incident power $P_{\rm in}$ and a parameter γ describing the fraction of incident power that is absorbed in the beam.

$$P_{\rm abs} = \gamma P_{\rm in} \text{Erf} \left(\frac{w \sqrt{\ln 2}}{\text{fwhm}} \right) \tag{7}$$

For example, for the constant-width array, a 500-nm-wide beam has 18% of the total optical power incident upon it, given the laser spot size. For the alternating-width array, the slightly larger focal width leads to a 500-nm-wide beam having 16% of the total power incident upon it. Figure 5b shows the measured maximum thermally induced frequency shift from Figure 4 as a function of beam width for the constant-width and alternatingwidth arrays. The frequency shift is stronger for narrower beams, as these have a lower heat capacity. The drawn lines are fits of eq 6 to the data, taking into account the width dependence of the incident power on the area of the beam (eq 7) and assuming a fixed fraction γ of the power incident on the beam to be absorbed in the beam. We find the data can be fitted well with this model for both constant- and alternatingwidth arrays and find that for a 500-nm-wide beam $P_{\rm abs} = 611$ $\mu\mathrm{W}$ for the constant-width array and P_{abs} = 396 $\mu\mathrm{W}$ for the alternating-width array.

Using the thermal frequency shift model, we find that for both the constant-width and alternating-width arrays, the sensitivity of frequency to absorbed power is, for a 500-nm-wide beam, $\delta f/P_{\rm abs}=6\%/{\rm mW}$. This is shown in Figure 5c, dividing out the focal width and power in Figure 5b. Because the heat capacity of a narrow beam scales with its width, the narrower beams are more sensitive to $P_{\rm abs}$. We find that the sensitivity to absorbed power is the same for both structures, as would be expected.

■ PARAMETRIC OSCILLATION OF NANOBEAMS

We have also studied the out-of-plane mechanical mode under high illumination power; Figure 6 shows the mechanical

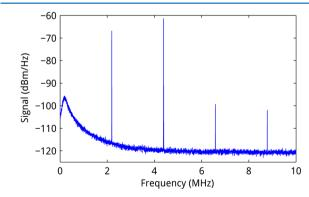


Figure 6. Mechanical response of a beam undergoing thermally induced parametric amplification, showing greatly increased response amplitude, high effective Q-factor, and higher order sidebands of the fundamental out-of-plane mode at 2.21 MHz.

resonance spectrum for an array of eight beams under 10 mW irradiation. The mechanical transduction amplitude exceeds the noise by 50 dB and is much more than in Figure 3. Also, the effective quality factor of the resonance increases to $Q_{\rm m} > 50.000$; this is a lower limit determined by thermal fluctuations that shift the resonance during the measurement averaging time. Figure 6 shows several harmonics at a frequency spacing exactly equal to the fundamental frequency of 2.21 MHz. The appearance of these higher order sidebands is intrinsic to the large modulation amplitude (up to 10% of the dc transmitted power). At these modulation amplitudes, power is transferred not only to the first sideband but also to higher order sidebands. Spectra such as that shown in Figure 6 are observed for laser powers > 8 mW, with the exact threshold depending on the laser focusing condition.

We attribute this behavior to parametric oscillations 17,21 that occur due to a driving force that is bolometric in nature: 25,33 for the out-of-plane mode, power absorbed in the beams causes an out-of-plane bending stress, due to the bilayer geometry of the beams and the differing thermal expansion coefficients $\alpha_{Si,N}$ and α_{Au} of silicon nitride and gold, which, if this stress is modulated at twice the mechanical frequency, can lead to parametric oscillations. When the out-of-plane displacement of one of the beams increases, the incoupling into the plasmonic resonance is reduced, reducing the heating and allowing the beam to cool off, with a certain time delay controlled by the heat capacity, restoring the equilibrium position. Then, light can be coupled back into the cavity, once again increasing absorption, driving the beams to greater and greater displacement. This process is eventually limited by coupling of mechanical energy into the higher harmonics of the system.

AVOIDED CROSSINGS IN ARRAYS OF BEAMS

Multiple mechanical oscillators can not only be used for parallelization of measurements. If the mechanical modes are coupled, a range of different effects can be observed and exploited, for instance using localized modes³⁴ to improve sensitivity³⁵ or using coupled resonances to create mechanical RF filters, ^{36,37} to enable single-input single-output mass sensing³⁸ or to observe synchronization.³⁹

If two resonators are coupled and then are tuned to make their eigenfrequencies match, their eigenfrequencies as a function of coupling will show an avoided crossing, as shown earlier for nanomechanical systems. Higure 7b shows a FEM simulation of the in-plane eigenmode of the fourth beam, showing that the neighboring beams also contribute to the eigenmode. To study the coupling between the beams, we fabricated an array of eight beams with beam widths leading to in-plane eigenfrequencies such that they could be thermally tuned to match. This was achieved by fabricating an array of eight beams with widths of 425, 450, 459, 480, 500, 525, 545, and 570 nm, where the second and third beams have nearly identical widths. The gap widths were fabricated to be alternating between 20 and 40 nm.

Figure 7a shows the measured mechanical transduction as a function of frequency and of the position of the focused laser beam in the array. The thermal tuning behavior observed in Figure 4 is clearly observed for four beams. Two avoided crossings are observed, indicated by the dashed outlines.

We also observe a nonavoided crossing, suggesting these mechanical modes are related to nonadjacent beams. For nonadjacent beams, we expect very low mechanical coupling

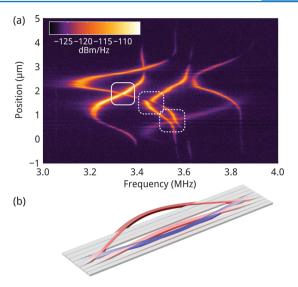


Figure 7. (a) Mechanical transduction spectrum of an array of eight microbeams, engineered to show avoided crossings in the thermally tuned eigenfrequencies of the microbeams. The widths of the beams were chosen such that one pair of neighboring beams would have similar eigenfrequencies. The dashed outlines indicate avoided crossings. The solid outline indicates a nonavoided crossing. (b) Simulated array of beams of increasing widths showing the shape of the fourth in-plane eigenmode, showing that the neighboring beams are also in motion due to the coupling at the anchoring points of the beams. Displacements are greatly exaggerated for clarity.

between these beams and, therefore, do not expect to see a splitting in the crossing.

CONCLUSION

We demonstrate parallel transduction of the thermally driven mechanical motion of an array of nanobeams using a simple free-space technique. The motion of each beam is transduced by the adjacent plasmonic slits. When these are identical, the transduction of in-plane motion can cancel, due to antisymmetric transduction by the slits. By tuning the gap width, the plasmonic resonances are tuned, allowing simultaneous parallel transduction of the mechanical modes of all beams.

The thermal tuning due to optical power absorption leads to resonance frequency shifts as large as 6%/mW of power absorbed in the beam. At powers above 8 mW parametric oscillations are observed due to a bolometric driving force. We find that neighboring beams are mechanically coupled through the membrane in which they are suspended. When thermally tuning such an array to make the eigenfrequencies of two neighboring beams match, the coupling between these beams creates an avoided crossing in the transduced mechanical modes of these two beams. The photothermoelastic effect observed in this work could therefore find application in tuning and actuating plasmonic micro- and nanomechanical resonators

The principle of parallel plasmonic mechanical transduction could be used in a variety of sensor array applications, due to its simple free-space readout and scalability to include many more resonators than shown here.

AUTHOR INFORMATION

Corresponding Author

*E-mail: verhagen@amolf.nl.

Notes

The authors declare no competing financial interest.

ACKNOWLEDGMENTS

This work is part of the research program of the "Stichting voor Fundamenteel Onderzoek der Materie" (FOM), which is financially supported by the "Nederlandse Organisatie voor Wetenschappelijk Onderzoek" (NWO). This work is also supported by the European Research Council.

REFERENCES

- (1) Ekinci, K. L.; Roukes, M. L. Nanoelectromechanical systems. *Rev. Sci. Instrum.* **2005**, *76*, 061101.
- (2) Li, M.; Tang, H. X.; Roukes, M. L. Ultra-sensitive NEMS-based cantilevers for sensing, scanned probe and very high-frequency applications. *Nat. Nanotechnol.* **2007**, *2*, 114–120.
- (3) Lifshitz, R.; Kenig, E.; Cross, M. C. Collective dynamics in arrays of coupled nonlinear resonators. In *Fluctuating Nonlinear Oscillators*; Dykman, M. I., Ed.; Oxford University Press, 2012; Chapter 11.
- (4) Mahboob, I.; Mounaix, M.; Nishiguchi, K.; Fujiwara, A.; Yamaguchi, H. A multimode electromechanical parametric resonator array. *Sci. Rep.* **2014**, *4*, 4448.
- (5) Waggoner, P. S.; Craighead, H. G. Micro- and nanomechanical sensors for environmental, chemical, and biological detection. *Lab Chip* **2007**, *7*, 1238–1255.
- (6) Datar, R.; Kim, S.; Jeon, S.; Hesketh, P.; Manalis, S.; Boisen, A.; Thundat, T. Cantilever sensors: nanomechanical tools for diagnostics. *MRS Bull.* **2009**, *34*, 449–454.
- (7) Arlett, J. L.; Myers, E. B.; Roukes, M. L. Comparative advantages of mechanical biosensors. *Nat. Nanotechnol.* **2011**, *6*, 203–215.
- (8) Bargatin, I.; Myers, E. B.; Aldridge, J. S.; Marcoux, C.; Brianceau, P.; Duraffourg, L.; Colinet, E.; Hentz, S.; Andreucci, P.; Roukes, M. L. Large-scale integration of nanoelectromechanical systems for gas sensing applications. *Nano Lett.* **2012**, *12*, 1269–1274.
- (9) Sadek, A. S.; Karabalin, R. B.; Du, J.; Roukes, M. L.; Koch, C.; Masmanidis, S. C. Wiring nanoscale biosensors with piezoelectric nanomechanical resonators. *Nano Lett.* **2010**, *10*, 1769–1773.
- (10) Truitt, P. A.; Hertzberg, J. B.; Huang, C. C.; Ekinci, K. L.; Schwab, K. C. Efficient and sensitive capacitive readout of nanomechanical resonator arrays. *Nano Lett.* **2007**, *7*, 120–126.
- (11) Yue, M.; Stachowiak, J. C.; Lin, H.; Datar, R.; Cote, R.; Majumdar, A. Label-free protein recognition two-dimensional array using nanomechanical sensors. *Nano Lett.* **2008**, *8*, 520–524.
- (12) Li, M.; Pernice, W. H. P.; Tang, H. X. Broadband all-photonic transduction of nanocantilevers. *Nat. Nanotechnol.* **2009**, *4*, 377–382.
- (13) Ou, J.-Y.; Plum, E.; Zhang, J.; Zheludev, N. I. An electromechanically reconfigurable plasmonic metamaterial operating in the near-infrared. *Nat. Nanotechnol.* **2013**, *8*, 252–255.
- (14) Thijssen, R.; Verhagen, E.; Kippenberg, T. J.; Polman, A. Plasmon nanomechanical coupling for nanoscale transduction. *Nano Lett.* **2013**, *13*, 3293–3297.
- (15) Miyazaki, H. T.; Kurokawa, Y. Squeezing visible light waves into a 3-nm-thick and 55-nm-long plasmon cavity. *Phys. Rev. Lett.* **2006**, *96*, 097401.
- (16) Eichenfield, M.; Camacho, R.; Chan, J.; Vahala, K. J.; Painter, O. A picogram- and nanometre-scale photonic-crystal optomechanical cavity. *Nature* **2009**, *459*, 550–555.
- (17) Kippenberg, T. J.; Rokhsari, H.; Carmon, T.; Scherer, A.; Vahala, K. J. Analysis of radiation-pressure induced mechanical oscillation of an optical microcavity. *Phys. Rev. Lett.* **2005**, *95*, 033901.
- (18) Jun, S. C.; Huang, X. M. H.; Manolidis, M.; Zorman, C. A.; Mehregany, M.; Hone, J. Electrothermal tuning of Al-SiC nanomechanical resonators. *Nanotechnology* **2006**, *17*, 1506.
- (19) Larsen, T.; Schmid, S.; Villanueva, L. G.; Boisen, A. Photothermal analysis of individual nanoparticulate samples using micromechanical resonators. *ACS Nano* **2013**, *7*, 6188–6193.
- (20) Schmid, S.; Wu, K.; Larsen, P. E.; Rindzevicius, T.; Boisen, A. Low-power photothermal probing of single plasmonic nanostructures

with nanomechanical string resonators. Nano Lett. 2014, 14, 2318-2321.

- (21) Yamada, S.; Schmid, S.; Larsen, T.; Hansen, O.; Boisen, A. Photothermal infrared spectroscopy of airborne samples with mechanical string resonators. *Anal. Chem.* **2013**, *85*, 10531–10535.
- (22) Metzger, C. H.; Karrai, K. Cavity cooling of a microlever. *Nature* **2004**, 432, 1002–1005.
- (23) Holscher, P. H; Milde; Zerweck, U.; Eng, L. M.; Hoffmann, R. The effective quality factor at low temperatures in dynamic force microscopes with Fabry-Pérot interferometer detection. *Appl. Phys. Lett.* **2009**, *94*, 223514.
- (24) Usami, K.; Naesby, A.; Bagci, T.; Nielsen, B. M.; Liu, J.; Stobbe, S.; Lodahl, P.; Polzik, E. S. Optical cavity cooling of mechanical modes of a semiconductor nanomembrane. *Nat. Phys.* **2012**, *8*, 168.
- (25) Zalalutdinov, M.; Zehnder, A.; Olkhovets, A.; Turner, S.; Sekaric, L.; Ilic, D. B.; Czaplewski; Parpia, J. M.; Craighead, H. G. Autoparametric optical drive for micromechanical oscillators. *Appl. Phys. Lett.* **2001**, *79*, 695.
- (26) Schmid, S.; Jensen, K. D.; Nielsen, K. H.; Boisen, A. Damping mechanisms in high-Q micro and nanomechanical string resonators. *Phys. Rev. B* **2011**, *84*, 165307.
- (27) Su, Y.-J.; Qian, C.-F.; Zhao, M.-H.; Zhang, T.-Y. Microbridge testing of silicon oxide/silicon nitride bilayer films deposited on silicon wafers. *Acta Mater.* **2000**, *48*, 4901–4915.
- (28) Bose, S.; Schmid, S.; Larsen, T.; Keller, S. S.; Sommer-Larsen, P.; Boisen, A.; Almdal, K. Micromechanical string resonators: analytical tool for thermal characterization of polymers. *ACS Macro Lett.* **2014**, *3*, 55–58.
- (29) Weaver, W.; Timoshenko, S.; Young, D. Vibration Problems in Engineering; John Wiley & Sons, 1990.
- (30) Chang, Y. A.; Himmel, L. Temperature dependence of the elastic constants of Cu, Ag, and Au above room temperature. *J. Appl. Phys.* **1966**, *37*, 3567–3572.
- (31) Rouxel, T.; Sanglebœuf, J.-C.; Huger, M.; Gault, C.; Besson, J.-L.; Testu, S. Temperature dependence of Young's modulus in Si_3N_4 -based ceramics: roles of sintering additives and of SiC-particle content. *Acta Mater.* **2002**, *50*, 1669–1682.
- (32) Schliesser, A.; Riviere, R.; Anetsberger, G.; Arcizet, O.; Kippenberg, T. J. Resolved-sideband cooling of a micromechanical oscillator. *Nat. Phys.* **2008**, *4*, 415–419.
- (33) Metzger, C.; Ludwig, M.; Neuenhahn, C.; Ortlieb, A.; Favero, I.; Karrai, K.; Marquardt, F. Self-induced oscillations in an optomechanical system driven by bolometric backaction. *Phys. Rev. Lett.* **2008**, *101*, 133903
- (34) Sato, M.; Hubbard, B. E.; Sievers, A. J.; Ilic, B.; Czaplewski, D. A.; Craighead, H. G. Observation of locked intrinsic localized vibrational modes in a micromechanical oscillator array. *Phys. Rev. Lett.* **2003**, *90*, 044102.
- (35) Spletzer, M.; Raman, A.; Sumali, H.; Sullivan, J. P. Highly sensitive mass detection and identification using vibration localization in coupled microcantilever arrays. *Appl. Phys. Lett.* **2008**, *92*, 114102.
- (36) Galayko, D.; Kaiser, A.; Legrand, B.; Buchaillot, L.; Combi, C.; Collard, D. Coupled-resonator micromechanical filters with voltage tuneable bandpass characteristic in thick-film polysilicon technology. *Sens. Actuators, A* **2006**, *126*, 227–240.
- (37) Nguyen, C.-C. MEMS technology for timing and frequency control. *IEEE Trans. Ultrason., Ferroelectr., Freq. Control* **2007**, *54*, 251–270.
- (38) DeMartini, B. E.; Rhoads, J. F.; Zielke, M. A.; Owen, K. G.; Shaw, S. W.; Turner, K. L. A single input-single output coupled microresonator array for the detection and identification of multiple analytes. *Appl. Phys. Lett.* **2008**, *93*, 054102.
- (39) Shim, S.-B.; Imboden, M.; Mohanty, P. Synchronized oscillation in coupled nanomechanical oscillators. *Science* **2007**, *316*, 95–99.
- (40) Buks, E.; Roukes, M. L. Electrically tunable collective response in a coupled micromechanical array. *J. Microelectromech. Syst.* **2002**, *11*, 802–807.
- (41) Okamoto, H.; Gourgout, A.; Chang, C.-Y.; Onomitsu, K.; Mahboob, I.; Chang, E. Y.; Yamaguchi, H. Coherent phonon

manipulation in coupled mechanical resonators. Nat. Phys. 2013, 9, 480-484.